

Phase and amplitude pulse shaping with two-dimensional phase-only spatial light modulators

Eugene Frumker* and Yaron Silberberg

Department of Physics of Complex Systems, Weizmann Institute of Science, Rehovot 76100, Israel

**Corresponding author: evgenyf@weizmann.ac.il*

Received August 29, 2007; accepted September 30, 2007;
posted October 8, 2007 (Doc. ID 86936); published November 9, 2007

We consider a programmable, phase, and amplitude femtosecond pulse shaper based on a two-dimensional (2D) reflective liquid-crystal (LC) spatial light modulator (SLM). A new zero-order pulse shaping scheme is introduced and compared to the first-order scheme, both theoretically and experimentally, using liquid crystal on silicon 2D SLM. While the spectral components of the pulse are spread across the horizontal dimension, we use the vertical direction for modulation of both spectral phases and amplitudes. It was found that while zero-order approach provided better light efficiency (67% versus 43%), the first-order scheme has superior dynamic range of amplitude modulation. © 2007 Optical Society of America

OCIS codes: 20.0320, 190.0190, 320.2250, 320.5540, 320.7160, 190.7110.

1. INTRODUCTION

Femtosecond Fourier-domain pulse shaping [1,2] has had a significant impact as an experimental tool and facilitated numerous exciting advances in many research fields. This technique, capable of accurate control of femtosecond optical waveforms, has enabled much progress in quantum coherent control [3,4], femtosecond microscopy and spectroscopy [5,6], nonlinear fiber optics [7], high harmonic generation [8] and others. A variety of techniques for applying dynamic Fourier-domain pulse shaping have been reported, such as liquid-crystal (LC) spatial light modulators (SLMs) [2], deformable mirrors [9], acousto-optic modulators [10], scanning over 2D mask [11], and electro-optical phased-array modulator [12].

It is often desirable to be able to control not only spectral phases, but also spectral amplitudes of the femtosecond pulse. This capability is particularly important for arbitrary waveform generation [13]. In principle, to achieve arbitrary temporal profiles, one has to control independently both spectral amplitudes and phases. Also, independent phase and amplitude spectral control can be useful in nonlinear spectroscopy and microscopy, for instance, in the spectral hole refilling technique [14] for use in tissue microscopy. In this application spectral amplitudes should be either completely blocked or a local oscillator (a few percent of the peak intensity) should be injected into the tailored spectral holes in a controlled way.

Amplitude modulation can be achieved with a single LC array with a polarizer by introducing light with appropriate input polarization relative to the LC axis. However, this also leads to coupled phase-modulation, which depends on the amplitude modulation level. Hence, for independent phase and amplitude control, two LC SLM arrays are used [13,15]. Although this advanced and efficient approach [13] is most popular today, it still has several inherent issues to be addressed. An extra modu-

lator is required with its circuitry, bulkiness, and very accurate mutual alignment between them. This usually doubles the system costs. Since the two modulators are physically separated (typically by several millimeters), the minimum single wavelength spot size is limited in order to ensure the Rayleigh range to be larger than this distance. Furthermore, the need for two polarizers results in additional losses and dispersion, and gratings used in the shaper exhibit significant polarization-dependent loss already. In principle, shapers based on acousto-optic modulators are capable of controlling both spectral phases and amplitudes; however, the acoustic grating wave, which fills the modulator's aperture, is not fixed. In spite of the fact that, for every single femtosecond pulse, the acoustic wave appears frozen on the time scale of propagation of that pulse through the modulator, the induced modulation grating changes significantly during the time between pulses of a typical mode-locked oscillator (~100 MHz). This practically limits the application of the acousto-optic shapers to lower-repetition-rate systems such as femtosecond amplifiers. Electro-optical phased array modulators may also provide independent control over spectral phases and amplitudes [12], and unsurpassed update rate on the nanosecond scale, but electro-optical materials such as gallium arsenide have a prohibitively high absorption at 800 nm, which makes them incompatible with very common Ti:sapphire femtosecond laser sources.

The advances in fabrication of 2D SLM, propelled by their application in displays, now offer new opportunities for pulse shaping. Recently, the diffraction-based (first-order) method for shaping both spectral phases and amplitude by use of 2D SLM was proposed by the Nelson group [16]. In this paper we introduce a new zero-order approach for complex-spectral phases and amplitude modulation. We also suggest an improvement for the first-

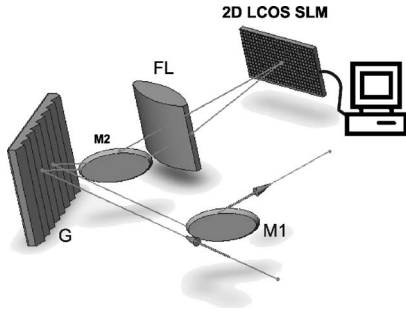


Fig. 1. Schematic of the 2D phase and amplitude SLM pulse shaper.

order technique, which will allow continuous spectral phase modulation versus discrete modulation [16]. The techniques are studied both theoretically and experimentally. In both cases a cylindrical lens is used as the Fourier lens (FL). Otherwise, the shaper layout is similar to a standard Fourier shaper in reflection geometry with the 2D SLM situated in the Fourier plane (Fig. 1) of the FL. The important aspects of angular orientation of the 2D SLM depend on the operation mode and will be discussed in Section 3. The use of a cylindrical lens ensures that each wavelength component, while focused in the horizontal direction at the Fourier plane, extends over a few millimeters in the vertical direction. While the spectral components of the pulse are spread across the horizontal plane, we use the vertical direction for modulation of both spectral phases and amplitudes. By writing a vertical phase grating in each column of the SLM's 2D matrix, we will achieve not only phase but also independent amplitude modulation control for the corresponding spectral component.

2. THEORETICAL CONSIDERATIONS

A. Zero-Order Approach

In the zero-order approach we encode the following phase function in vertical direction for each spectral component ω :

$$T(z, \omega) = \left[\text{rect}\left(\frac{z}{2z_0}\right) \cdot e^{i(A(\omega)\text{rect}\left(\frac{z}{z_0}\right) + B(\omega))} \right] * \sum_{n=-\infty}^{+\infty} \delta(z - 2z_0n). \quad (1)$$

The complex transmittance $T(z, \omega) = e^{i\Phi(z, \omega)}$ is a periodic function with period $P = 2z_0$. Using Fourier decomposition in vertical (z) direction, one can write

$$T(z, \omega) = \sum_{n=-\infty}^{+\infty} C_n e^{i\frac{2\pi n}{P}z}. \quad (2)$$

The zero diffraction order of this phase grating corresponds to the zero-order in the Fourier expansion and is simply an average of the transmittance (1):

$$C_0(\omega) = \frac{1}{2z_0} \int_{-z_0}^{z_0} T(z, \omega) dz = \frac{1}{2} (1 + e^{iA(\omega)}) e^{iB(\omega)}. \quad (3)$$

The intensity of this zero diffraction order is given by

$$I_0 \sim |C_0(\omega)|^2 = \cos^2\left(\frac{A(\omega)}{2}\right). \quad (4)$$

We see that the amplitude modulation is solely determined by $A(\omega)$. Note that a full dynamic range of amplitude modulation of every frequency component is, in principle, possible by varying the $A(\omega)$ from 0 (no amplitude attenuation) to π (complete blockage) regardless of the value of $B(\omega)$. For a desired amplitude modulation $\tau(\omega)$, and phase modulation $\varphi(\omega)$, and for a specific frequency component ω , the $A(\omega)$ and $B(\omega)$ can be determined from

$$A(\omega) = 2 \arccos[\tau(\omega)], \quad (5)$$

$$B(\omega) = \varphi(\omega) - \arg(1 + e^{iA(\omega)}) = \varphi(\omega) - \frac{A(\omega)}{2}. \quad (6)$$

Examples of 2D SLM phase map encoding for purely amplitude and purely phase modulation in the proposed zero-order approach are shown in Figs. 2(c) and 2(d), respectively. Pure phase modulation of a specific frequency component ω_0 corresponds to uniform phase encoding into 2D SLM along the vertical direction of the SLM [Fig. 2(d)]. Pure amplitude modulation is achieved by encoding phase grating along vertical direction for specific frequency component as shown in Fig. 2(c). We note that even if one wants to get pure amplitude modulation [$\varphi(\omega) = 0$], $B(\omega)$ still has to be introduced to compensate for the "parasitic" phase accompanied by amplitude modulation [$B(\omega) = -A(\omega)/2$].

B. First-Order Approach

In this approach a blazed phase grating is encoded into the SLM to provide maximum efficiency in the first diffraction order, which is used for forming the output pulse.

Let us take a closer look at this case. In the first-order approach we encode the following phase function in vertical direction for each spectral component:

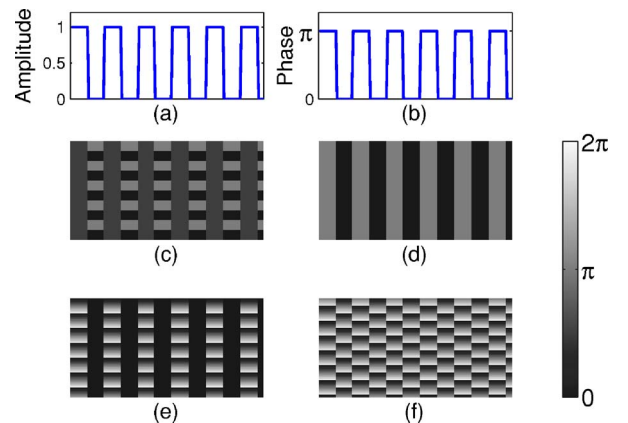


Fig. 2. (Color online) Example of actual 2D phase encoding into the SLM. (a) Periodic amplitude-only modulation. (b) Periodic phase-only modulation. (c) and (d) Zero-order mask encoded for amplitude only (c) and phase only (d). (e) and (f) First-order mask encoded for amplitude only (e) and phase only (f).

$$T(z, \omega) = \left[e^{i\left(\frac{2\pi\alpha(\omega)}{P}z + \pi\right)} \cdot \text{rect}\left(\frac{z}{P}\right) \right] * \sum_{n=-\infty}^{+\infty} \delta(z - nP) * \delta(z - s(\omega)), \quad (7)$$

where the expression in the square brackets stands for the single period blazing form factor of the grating, convolution with the infinite sum of the delta functions stands for the periodic continuation of the grating form factor in the vertical direction, and convolution with the $\delta(z - s(\omega))$ accounts for the intentionally introduced grating shift for the ω -frequency component. To take into account the finite beam extension we multiply the infinitely extended $T(z, \omega)$ in Eq. (7) by an apodization factor (typically of Gaussian profile)— $A(z/D)$.

The Fourier transform of the blazed form factor is

$$E_{\text{form}}(k_z, \omega) \propto \text{sinc}\left(\frac{k_z}{1/P}\right) * \delta(k_z - \alpha(\omega)/P). \quad (8)$$

Let us perform the plane wave decomposition in vertical plane ($z \leftrightarrow k_z$)

$$E(k_z, \omega) \propto \left\{ \text{sinc}\left(\frac{k_z - \alpha(\omega)/P}{1/P}\right) \cdot e^{i2\pi s(\omega)k_z} \times \sum_{n=-\infty}^{+\infty} \delta(k_z - n/P) \right\} * \tilde{A}\left(\frac{k_z}{1/D}\right). \quad (9)$$

For the first-order ($n=1$) we have

$$E^{+1}(k_z, \omega) \propto \text{sinc}[1 - \alpha(\omega)] \cdot e^{i\frac{2\pi s(\omega)}{P}} \cdot \tilde{A}\left(\frac{k_z - 1/P}{1/D}\right), \quad (10)$$

where D is the finite beam extension, and $\alpha(\omega) \leq 1$ is the blazing dynamic range value.

Control over $\alpha(\omega)$ will be used to encode the desirable amplitude modulation. Control of the phase is somewhat more complex in this case. Moving the blazed grating in a vertical direction produces the phase shift of the diffracted light up to 2π value. Because of the discrete nature of the pixels the required continuous control of the phase is impossible by the grating shift alone. For example, in the case of four pixels per blazing period we get $2\pi/4$ phase jumps moving the grating vertically by a minimum possible of one pixel. Since the device can supply more than 2.5π ($\Phi_{\text{max}} \geq 2.5\pi$) of dynamic range for our wavelength of ~ 800 nm, we use the “extra” $\sim \pi/2$ modulation to achieve continuous phase control by combining a shift in the grating with this additional phase. Specifically, the desired phase $\varphi(\omega)$ should be quantized modulus $2\pi/N$ (where N is a number of pixels per period) that is encoded via the vertical grating position, and the residual part will be encoded via the phase added to the blazed grating by SLM. The necessary condition for implementation of this scheme is that the extra modulation over 2π provided by SLM should be larger than the quantization phase step by grating shift

$$\Phi_{\text{max}}(\omega) - 2\pi \geq \frac{2\pi}{N} \quad \forall \omega. \quad (11)$$

From Eq. (8) it follows that continuous blazed grating has the property that, if the peak-to-peak phase variation it introduces is exactly 2π radians, then 100% of the incident light will be diffracted into a single first diffraction order. In practice our SLM is composed of discrete pixels. The overall diffraction efficiency of the q th order for such a pixelized structure is analogous to binary optics approximation and is given by [17]

$$\eta_q = \text{sinc}^2\left(\frac{q}{2^N}\right) \frac{\text{sinc}^2\left(q - \frac{\Phi_0}{2\pi}\right)}{\text{sinc}^2\left(\frac{q - \frac{\Phi_0}{2\pi}}{2^N}\right)}, \quad (12)$$

where Φ_0 is the peak-to-peak phase difference of the continuous blazed grating. For example, with four quantization levels ($N=2$), which is reasonable in our case, one can estimate a theoretical attainable efficiency of about 80%.

3. EXPERIMENTAL RESULTS

The experiments were carried out with a home-built Ti:sapphire oscillator followed by prism compressor to compensate for residual chirp. The oscillator was centered at about 800 nm with about 30 nm full width half maximum (FWHM) bandwidth. The average output power before the compressor was about 250 mW and a repetition rate of ~ 100 MHz. A 50% beam splitter was mounted after the prism compressor to split the beam between the shaper and reference arm for cross-correlation. In the pulse shaper, schematically shown in Fig. 1, the incident beam is diffracted at nearly Littrow angle by reflective silver coated diffraction grating G (1200 mm^{-1}). The folding mirror M2 directs the diffracted beam into singlet cylindrical FL ($f=100$ mm). The LC on silicon (LCOS) 2D SLM was placed in the Fourier plane of the lens. We used a Holoeye Photonics AG HEO1080P phase only high definition television (HDTV) developer kit as our SLM. The LCOS panel measures 15.36×8.64 mm active area and has $1920(\text{horizontal}) \times 1080(\text{vertical})$ pixels. It has $8 \mu\text{m}$ pixel to pixel distance and better than 87% pixel area filling factor. The device uses nematic electronically controlled birefringence (ECB) mode LC type, ensuring continuous phase modulation.

The SLM was calibrated with a home-built Michelson type interferometer. The 2D SLM area was divided into two equal parts. The upper part was addressed with a particular gray scale value, while the lower part was left intact. The interference fringes shift was recorded and corresponding phase value retrieved. In this interferometric setup it was also observed that the SLM is not perfectly flat, but rather has a slightly concave surface with about six to seven concentric fringes at 633 nm across the horizontal direction of the active area of the SLM, which corresponds to radius of curvature of about 25 m. This causes a slight quadratic phase induced on the shaped pulse, but can be easily compensated for by shifting the

SLM from exact $4-f$ configuration. It was experimentally verified that with horizontal polarization incident of the device, no noticeable parasitic amplitude modulation was observed. Given the shaper parameters, we expect about 0.06 nm/pixel resolution in near Littrow operation mode. This estimation was experimentally confirmed by repeatedly encoding a phase step along the SLM in different pixel positions and looking into spectral dips due to diffraction at the phase step. This way we also accurately established pixel to wavelength correspondence, which was used for spectral phase calculations and encoding across the SLM in the shaper. The single wavelength spot size in the Fourier plane was $\sim 30 \mu\text{m}$ in horizontal and $\sim 3 \text{mm}$ in vertical direction.

A. Zero-Order Operation

In the zero-order operation mode, the SLM is positioned perpendicular to the horizontal plane of the shaper, but it is tilted by a small angle around the vertical axis to allow the shaped beam outgoing from the shaper to be intercepted by mirror M1. In the paraxial approximation, this tilt is equivalent to a linear spectral phase in the Fourier plane, or to a distortionless time shift of the output signal in the time domain. Actually a fast-scanning delay line was previously built with a similar system, but in the Fourier plane a simple scanning mirror [18,19] was placed instead of SLM. It was measured that LCOS 2D SLM efficiency in the zero order is $\sim 67\%$.

To investigate the amplitude modulation capability of the shaper, the output beam from M1 was directed into an optical spectrum analyzer (OSA) Ando AQ-6315A. Different spectral amplitudes were applied to the 2D SLM with no spectral phase modulation according to Eqs. (5) and (6), and corresponding spectral intensities were recorded by an OSA. The modulation period in vertical direction $P=2z_0$ was set to be 12 pixels ($96 \mu\text{m}$).

Examples of spectral intensity for periodic binary amplitude spectral modulations [as in Fig. 2(a)] with periods of 6.2 THz and 3.1 THz are shown in Figs. 3(a) and 3(b),

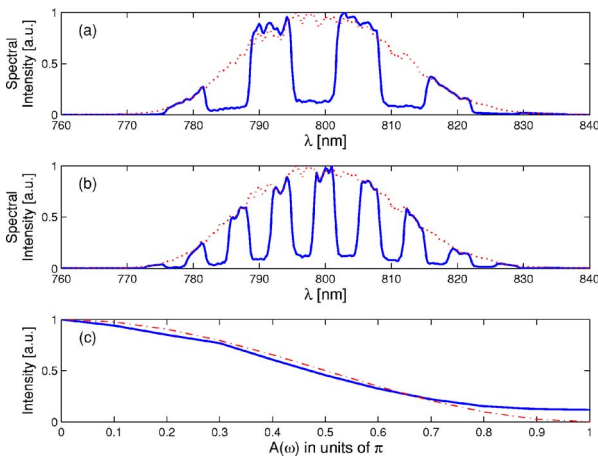


Fig. 3. (Color online) Experimental results of amplitude modulation in the zero-order approach. (a) and (b) Periodic binary spectral amplitude modulation with a period of 6.2 THz and 3.1 THz, respectively. Solid line—spectral amplitude modulation applied. Dotted line—no modulation applied. (c) Amplitude modulation versus $A(\omega)$ encoded. Solid line—experimental result. Dashed-dotted line—theoretical expectation.

respectively. Despite the fact that in the target amplitude function the minimum value was set to 0 (i.e., complete blockage of correspondent spectral components), we can clearly see in the experimental data that the spectral intensity does not vanish. Further, we encoded the spectral amplitude step function at about spectral center 800 nm into the SLM with different values of $A(\omega)$ in Eq. (1). In Fig. 3(c) both theoretical and experimentally measured spectral intensity modulation is shown. The experimental data are presented after averaging over 180 spectral data points for each value of $A(\omega)$ to reduce the random noise. Up to the $A(\omega) \cong 0.7\pi$ we see very good agreement between theoretical and measured values, but when $A(\omega)$ approaches π , the experimental measured intensity does not go below 11.6%, while theoretically it should vanish. We experimentally verified that the maximum spectral intensity attenuation was indeed achieved for $A(\omega) = \pi$, thereby eliminating the possibility of calibration errors.

The nonideal blocking of the device was associated with “dead zones” and a parasitic time-dependent modulation of the device. To study this important issue in more detail we examined amplitude modulation in the time domain. The whole SLM was set to provide equal spectral intensity attenuation for all frequencies, and the output was monitored with a New Focus Model 2033 nanosecond photodetector and a Tektronix TDS 5034 oscilloscope. In Fig. 4 we can see output intensity for different $A(\omega)$. Trace (a) was recorded with no phase applied. A constant signal is obtained, accompanied by a small amount of noise. At the same time, for $A(\omega) = \pi$, the minimum signal is achieved, which is significantly modulated in the time domain with a characteristic frequency of $\sim 300 \text{Hz}$. The minimum is at 11% of modulated output, while maximum spikes reach 20%, which corresponds to 0.29 in the undesired modulation contrast. The problem persists also for other values of $A(\omega)$. Specifically, for $A(\omega) = \pi/2$ [Fig. 4 trace (b)], the minimum reflectivity is 35% of output, with maximum peaks to 59%, which corresponds to 0.25 in this parasitic modulation contrast. Although the modulation frequency remains the same $\sim 300 \text{Hz}$, the temporal modulation profile is clearly different. It turned out that this “flicker” problem is the result of the electronic modulation scheme

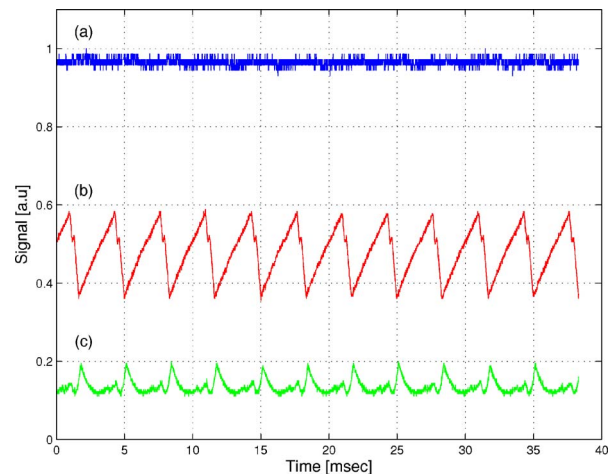


Fig. 4. (Color online) Experimentally observed flicker. (a) No phase is applied. (b) $A(\omega) = \pi/2$ applied for all ω . (c) $A(\omega) = \pi$ applied for all ω .

applied by the manufacturer in the device, and is not a real physical limitation of the LCOS display technology. This problem is not the only reason for residual amplitude modulation in the zero-order operation scheme. There are dead zones present between the active area of the pixels, which according to manufacturer's specifications account for about 13% of the total 2D SLM area. These dead zones may scatter light into the zero-order, however, due to their periodic structure, the dead zones in general diffract light into all orders (depending on the form factor of the individual scatterer). Their effect can be completely canceled by proper tuning of $A(\omega)$ and $B(\omega)$. If dead zone grating produces some diffraction into zero order with definite phase φ_{DZ} and amplitude τ_{DZ} , it can be canceled out by letting $A=2\arccos(\tau_{DZ})$ and $B=-\varphi_{DZ}-A/2$ as follows from Eqs. (5) and (6). We did not observe experimentally the reduction of residual amplitude modulation following this procedure. One possible reason could be that dead zone regions are not optically flat enough. This issue is interesting for future investigations. As the measured spectral intensity is proportional to the integral average of the temporal trace, we can estimate that for our LCOS 2D SLM $\sim 20\%$ of the parasitic residual amplitude modulation is due to the flicker problem and $\sim 80\%$ due to the uncompensated dead zones contribution.

To test the shaping capability in the zero-order operation, we encoded different periodic phase and amplitude functions following the procedure described in Subsection 2.A.

The output from the shaper was directed via chopper into the signal arm of noncollinear cross correlator. The reference unshaped beam sampled by 50% beam splitter and signal beam were focused by a spherical mirror ($f = 100$ mm) into $20\ \mu\text{m}$ β -barium borate (BBO) crystal, and the second harmonic signal was filtered and detected by a photomultiplier tube [(PMT) Hamamatsu model 1P28] and fed into a lock-in amplifier (Signal Recovery 7265) referenced to the chopper modulation frequency. Typical results are shown in Fig. 5. Figure 5(a) shows a cross correlation result with no modulation applied on the SLM.

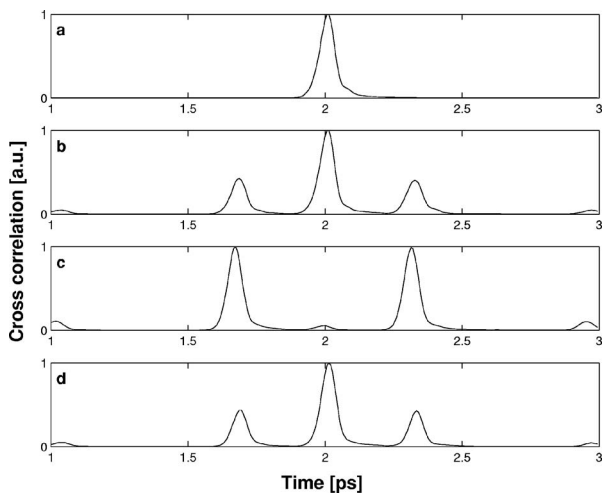


Fig. 5. Experimental results for cross correlation for zero-order approach. (a) No phase is applied. (b) Periodic phase-only modulation with binary modulation depth of $\pi/2$ and period 3.1 THz. (c) Periodic phase-only modulation with modulation depth of π . (d) Periodic amplitude-only modulation.

The cross correlation pulse width is practically Fourier limited with a slightly asymmetric tail indicating some small residual third order spectral phase. In Fig. 5(b) the cross correlation result is shown for binary periodic phase only modulation, similar to the ones shown in Figs. 2(b) and 2(d), but with phase modulation depth of $\pi/2$. Such periodic phase modulation should produce a series of pulses with vanishing even temporal orders. This relative amplitude distribution is further apodized as a result of the finite spot size in the Fourier plane [1]. In Fig. 5(b) the three central cross correlation peaks are due to the zero and first temporal orders. The small peaks seen at the beginning and the end of the picture are due to the third temporal order as the second order vanishes. The period of this modulation was 3.1 THz and the distance between zero-order and first-order temporal satellites was measured ~ 320 fs as expected. In Fig. 5(c) cross correlation trace is shown for the same phase only periodic spectral mask, but with a modulation depth of π . For this modulation depth one would expect complete cancellation of the temporal zero-order replica ($I_0 \sim \cos^2(\varphi/2)$, where I_0 is the intensity of temporal zero-order, and φ is the phase modulation depth) in the time domain. In Fig. 5(c) we can clearly see that residual temporal zero-order pulse replica persists in the time domain. The height of this temporal zero-order peak in the cross correlation trace is about 0.05 of the first-order peak. It means that, at most, 2.5% of the total intensity goes to the first-order (even neglecting higher than first order temporal satellites). That is of the same order of the flicker contribution to the amplitude modulation. This indicates that dead zones do not contribute to the temporal zero order in the cross correlation trace. In Fig. 5(d) the cross correlation result is shown for binary periodic amplitude only modulation, as in Figs. 2(a) and 2(c). This periodic amplitude modulation should result in a series of pulses similar to the phase only modulation case, but with relative intensities proportional now to $\text{sinc}^2(n/2)$ for the n th-temporal order pulse, further apodized as the result of the finite spot size. In Fig. 5(d) we see that even temporal orders vanish, as follows from analytical prediction, and the experimentally measured first and third temporal orders have intensity 0.42 and 0.045 relative to the zero-order intensity— in very good argument with theoretically expected results. Note that in the case of amplitude modulation the temporal zero-order amplitude is always larger than that of higher temporal orders, while in the periodic phase modulation case the energy distribution between zero and higher temporal orders can be continuously controlled up to complete vanishing of the zero-order pulse as in Fig. 5(c). It is also clear that in an amplitude modulation case the total intensity is attenuated, while for phase modulation the intensity is preserved.

B. First-Order Operation

In the first-order mode the SLM is not only tilted by a small angle around a vertical axis to allow the shaped beam outgoing from the shaper to be intercepted by mirror M1 (Fig. 1), but it is also tilted about the horizontal axis to allow the first diffraction order of the encoded blazed grating to be in the horizontal plane of the optical shaper. In the outlined experiments, the blazing period

was chosen to be 8 pixels ($64 \mu\text{m}$). Theoretically this eight multilevel step approximation should provide about 95% of diffraction efficiency into the first-order according to Eq. (12). In practice, it was measured that LCOS 2D SLM light efficiency in the first-order operation mode of the shaper is $\sim 43\%$. We estimate that absorption and scattering in the LC layer of the SLM, dead zones, absorption in the backplane of LCOS, flicker problem, and imperfections in the exact blazed phase realization are among the main factors that limit the practically achievable diffraction efficiency.

To study the amplitude modulation capability in the first-order operation mode, the output beam from M1 was fed into the OSA. Different spectral amplitudes were applied to the 2D SLM with no spectral phase modulation according to Eq. (10), and corresponding spectral intensities were recorded by the OSA. Typical examples of spectral intensity for periodic, binary amplitude spectral modulations with periods of 6.2 THz and 3.1 THz are shown in Figs. 3(a) and 3(b), respectively.

Contrary to the zero-order operation mode, we can see that for the blocked spectral amplitudes there is no visible leakage of energy. We measured the varying amplitude attenuation changing the $\alpha(\omega)$. The data, averaged over 80 spectral sampling points, are shown in Fig. 6(c). In fact, when zero spectral amplitude was set in the first-order operation [$\alpha(\omega)=0$], the corresponding residual spectral amplitude intensity was below the noise level of our spectral measurement apparatus. To measure the full amplitude modulation dynamic range we replaced the optical fiber of the OSA with an Ophir Laserstar PD300 detector. Then we operated the shaper in an on/off (all spectral amplitudes allowed or all of them blocked) regime. We measured better than 2800:1 contrast ratio. To check the spectral resolution of the shaping apparatus, the spectral amplitude edge was applied in the middle of the spectrum, and the resulting spectrum was recorded with an OSA at 0.5 \AA resolution. The spectral rise step

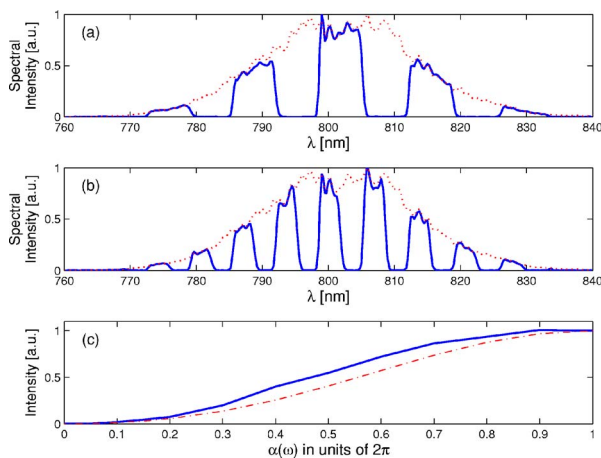


Fig. 6. (Color online) Experimental results of amplitude modulation in the first-order approach. (a) and (b) Periodic binary spectral amplitude modulation with period of 6.2 THz and 3.1 THz, respectively. Solid line—spectral amplitude modulation applied. Dotted line—no modulation applied. (c) Amplitude modulation versus blazing multiplier factor— $\alpha(\omega)$ encoded. Solid line—experimental result. Dashed-dotted line—theoretical expectation.

(10%–90%) was found to be $\sim 0.4 \text{ nm}$, which is very close to the diffraction limit resolution, given the incident beam width ($\sim 3 \text{ mm}$), the parameters of our FL, and the diffraction grating.

We took advantage of this impressive amplitude modulation to carry out spectral “two slit” experiments. In typical experiments, all spectral amplitudes were blocked in the Fourier plane of our shaper, except for two narrow (1.5 nm each) spectral slits separated by 5 nm center-to-center distance as shown in Fig. 7(a).

The experimentally measured cross correlation temporal trace, where no relative phase is applied between the two slits is shown in Fig. 7(b). The periodic ($\sim 420 \text{ fs}$ period) signal bound by $\sim 1250 \text{ fs}$ temporal envelope are in excellent agreement with theoretically expected values for the slit’s width and distance between the slits, respectively. In Fig. 7(c) the cross correlation temporal trace is shown for the same slit parameters, but with π spectral phase applied between two slits. One can clearly see that it resulted in the envelope shift by half of the period, as expected.

Another important issue to be addressed is the choice of the blazing period. The smaller the blazing period, the larger the angular separation between the first and zero order, and consequently, the lower the level of stray light scattered or diffracted into the useful first order. This is a critical advantage considering that high spectral amplitude blocking is the main advantage of the first order over the zero order operation scheme. On the other hand, the first order modulation scheme features inherent spectral angular chirp in the vertical direction. This chirp $\delta\alpha$ is proportional to $\delta\alpha \sim \delta\lambda / (P \cos \alpha)$, where P is the blazing period and α is the first order diffraction angle; thus a larger blazing period would result in lower amounts of angular spectral chirp. It is also important to note that a larger blazing period requires less “extra” 2π phase modulation of the SLM to ensure the continuous spectral phase modulation capability suggested in Subsection 2.B [Eq. (11)]. In fact even if 2D SLM would not be able to provide 2π dynamic range, it still could be possible to achieve

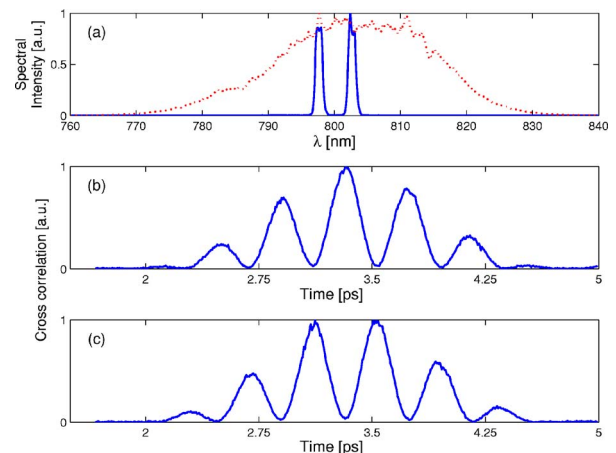


Fig. 7. (Color online) Experimental results of “two spectral slit” experiment in the first-order approach. (a) Dotted line—nonmodulated spectra. Solid line—two spectral slit was applied. Slit full width—1.5 nm, distance between the centers of the slits—5 nm. (b) Cross correlation with no phase was applied. (c) Cross correlation with π phase step applied between the slits.

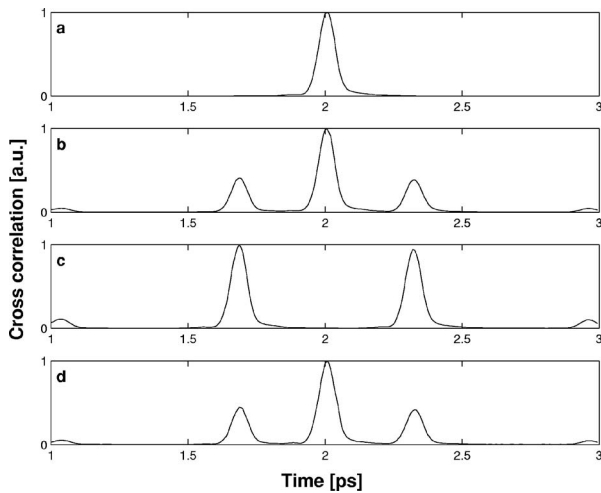


Fig. 8. Experimental results for cross correlation for first-order approach. (a) No phase is applied. (b) Periodic phase-only modulation with binary modulation depth of $\pi/2$ and period 3.1 THz. (c) Periodic phase-only modulation with modulation depth of π . (d) Periodic amplitude-only modulation.

the discrete (with number of controlled spectral phase levels given by number of SLM pixels per blazing period) control of spectral phases with full 2π dynamic range, although the diffraction efficiency in this case would be reduced.

As in the case of zero order modulation scheme, we check the pulse shaping capability by encoding different periodic phase and amplitude functions following the procedure outlined in Subsection 2.B. The cross correlation results are shown in Fig. 8. Figure 8(a) shows the cross correlation trace with no modulation. The cross correlation pulse width is practically Fourier limited. The same good agreement between theoretical expectation and experimental results was found for periodic binary phase-only [Fig. 8(b)] and amplitude-only modulation [Fig. 8(d)]. It is important to note that in periodic binary π phase depth modulation, there is no residual zero order temporal modulation [Fig. 8(c)], as theoretically expected. That is contrary to the zero order modulation scheme, when a small zero order temporal replica was experimentally evident, corresponding very closely to the amount of flicker observed in the device. In the first order modulation scheme, the flicker would cause temporal modulation (following the flicker temporal pattern) of the efficiency of the shaping apparatus, sending the light into blocked zero order.

4. CONCLUSION

We have studied, both theoretically and experimentally, phase and amplitude femtosecond pulse shaping based on a 2D LC SLM. Zero-order approach was introduced, theoretically analyzed, and experimentally proven to have significantly higher light efficiency than first order approach and being inherently free of vertical angular frequency chirp. Continuous spectral phase modulation scheme in the first-order operation was suggested. We believe that amplitude modulation dynamic range in the zero-order scheme can be further improved, at least by an additional order of magnitude, by improving the optical quality of 2D

SLM and solving the flicker problem that limits current devices. Our experimental data proved that both zero- and first-order techniques have excellent pulse shaping, accuracy, and fidelity.

In general, we can consider zero- and first-order techniques as two complementary schemes with unique advantages and disadvantages—the zero-order method should be used when light efficiency is of major importance, while first-order techniques should be adopted in applications when amplitude modulation dynamic range is of main concern. In future studies, given the superior pixel count and constantly improving quality of modern 2D SLM modulators, these techniques can be combined with scanning shaping methods [20] to achieve both arbitrary waveform generation and significantly enhanced update rate. We believe that a complex (phase and amplitude) modulation technique with 2D SLM, in addition to other previously introduced methodologies [20–22] of using the 2D SLM in pulse shaping, will prompt the active usage of 2D modulators in a variety of ultrafast science frontiers.

ACKNOWLEDGMENTS

The authors are very grateful to Eran Tal for helpful discussions. This work was supported by grants from Israel Science Foundation and the Yeshaya Horowitz foundation.

REFERENCES

1. A. M. Weiner, "Femtosecond pulse shaping using spatial light modulators," *Rev. Sci. Instrum.* **71**, 1929–1960 (2000).
2. A. M. Weiner, D. E. Leaird, J. S. Patel, and J. R. Wullert II, "Programmable femtosecond pulse shaping by use of a multielement liquid-crystal phase modulator," *Opt. Lett.* **15**, 326–328 (1990).
3. A. Assion, T. Baumert, M. Bergt, T. Brixner, B. Kiefer, V. Seyfried, M. Strehle, and G. Gerber, "Control of chemical reactions by feedback-optimized phase-shaped femtosecond laser pulses," *Science* **282**, 919–922 (1998).
4. D. Meshulach and Y. Silberberg, "Coherent quantum control of two-photon transitions by a femtosecond laser pulse," *Nature* **396**, 239–242 (1998).
5. P. Tian, D. Keusters, Y. Suzuki, and W. S. Warren, "Femtosecond phase-coherent two-dimensional spectroscopy," *Science* **300**, 1553–1555 (2003).
6. N. Dudovich, D. Oron, and Y. Silberberg, "Single-pulse coherently-controlled nonlinear raman spectroscopy and microscopy," *Nature* **418**, 512–514 (2002).
7. A. Efimov, A. J. Taylor, F. G. Omenetto, and E. Vanin, "Adaptive control of femtosecond soliton self-frequency shift in fibers," *Opt. Lett.* **29**, 271–273 (2004).
8. R. Bartels, S. Backus, E. Zeek, L. Misoguti, G. Vdovin, I. P. Christov, M. M. Murnane, and H. C. Kapteyn, "Shaped-pulse optimization of coherent emission of high-harmonic soft x-rays," *Nature* **406**, 164–166 (2000).
9. E. Zeek, K. Maginnis, S. Backus, U. Russek, M. Murnane, G. Mourou, H. Kapteyn, and G. Vdovin, "Pulse compression by use of deformable mirrors," *Opt. Lett.* **24**, 493–495 (1999).
10. C. W. Hillegas, J. X. Tull, D. Goswami, D. Strickland, and W. S. Warren, "Femtosecond laser pulse shaping by use of microsecond radio-frequency pulses," *Opt. Lett.* **19**, 737–739 (1994).
11. E. Frumker, D. Oron, D. Mandelik, and Y. Silberberg, "Femtosecond pulse-shape modulation at kilohertz rates," *Opt. Lett.* **29**, 890–892 (2004).
12. E. Frumker, E. Tal, Y. Silberberg, and D. Majer,

- “Femtosecond pulse-shape modulation at nanosecond rates,” *Opt. Lett.* **30**, 2796–2798 (2005).
13. M. M. Wefers and K. A. Nelson, “Generation of high-fidelity programmable ultrafast optical waveforms,” *Opt. Lett.* **20**, 1047–1049 (1995).
 14. M. C. Fischer, T. Ye, G. Yurtsever, A. Miller, M. Ciocca, W. Wagner, and W. S. Warren, “Two-photon absorption and self-phase modulation measurements with shaped femtosecond laser pulses,” *Opt. Lett.* **30**, 1551–1553 (2005).
 15. M. M. Wefers and K. A. Nelson, “Programmable phase and amplitude femtosecond pulse shaping,” *Opt. Lett.* **18**, 2032–2034 (1993).
 16. J. C. Vaughan, T. Hornung, T. Feurer, and K. A. Nelson, “Diffraction-based femtosecond pulse shaping with a 2D SLM,” *Opt. Lett.* **30**, 323–325 (2005).
 17. J. W. Goodman, *Introduction to Fourier Optics* (McGraw-Hill, 1996).
 18. K. Kwong, D. Yankelevich, K. Chu, J. Heritage, and A. Dienes, “400 Hz mechanical scanning optical delay line,” *Opt. Lett.* **18**, 558–560 (1993).
 19. G. J. Tearney, B. E. Bouma, and J. G. Fujimoto, “High-speed phase- and group-delay scanning with a grating-based phase control delay line,” *Opt. Lett.* **22**, 1811–1813 (1997).
 20. E. Frumker and Y. Silberberg, “Femtosecond pulse shaping using a 2D liquid crystal spatial light modulator,” *Opt. Lett.* **32**, 1384–1386 (2007).
 21. T. Feurer, J. C. Vaughan, R. M. Koehl, and K. A. Nelson, “Multidimensional control of femtosecond pulses by use of a programmable liquid-crystal matrix,” *Opt. Lett.* **27**, 652–654 (2002).
 22. T. Feurer, J. C. Vaughan, and K. A. Nelson, “Spatiotemporal coherent control of lattice vibrational waves,” *Science* **299**, 374–377 (2003).